Check for updates

DNA hairpin base-flipping dynamics drives APOBEC3A recognition and selectivity†

Mark A. Hix, [ID] [a] A. G. Pramoda Sahankumari, [ID] [a] Ashok S. Bhagwat [ID] [ab] and Alice R. Walker [ID] *[a]

APOBEC3A is a deoxycytidine deaminase which acts preferentially upon a 5'-TC-3' motif, and was recently shown to prefer hairpin loops over unstructured single-stranded DNA. However, the underlying molecular details for its substrate specificity remain unclear. In this work we apply classical molecular dynamics to 212 unique hairpin loops in solvent, with lengths of 3 and 4 nucleotides in the loop, and a representative subset of 23 bound to APOBEC3A. This allows us to gain statistical insight into the types of motions and sequences potentially important for APOBEC3A activity. We demonstrate that base-flipping occurs in solvent before binding to APOBEC3A semi-dependent on the hairpin loop sequence, and that binding does not necessarily require the presence of a cytosine on the hairpin loop. Furthermore, we show measurable physical metrics, such as RMSD and sugar puckering, which may aid in identifying sequences which will exhibit higher rates of base-flipping commensurate with increased APOBEC3A activity.

1. Introduction

The APOBEC3 family of enzymes are deoxycytidine deaminases which catalyze the deamination reaction of deoxycytidine into uracil in single-stranded DNA (ssDNA) as part of a number of important biological processes including immune response, epigenetic regulation, and anti-viral cellular activity.[1–4] Members of the APOBEC3 family have a conserved subunit structure consisting of five β-sheets surrounded by six α-helices.[4]

APOBEC3s are known to exhibit preferential binding to 5'-TC-3' motifs.[5–10] The physical driver behind the recognition mechanism for specific sequences by individual members of the APOBEC3 family is under ongoing study. The specific amino acids on loop 7 have been shown to interact favorably with specific cytosine-containing motifs.[6,7,10–13] It has also been shown that APOBEC3s preferentially act upon hairpin loops (HPLs) of ssDNA, which allow the target cytosine to be more exposed and easier to bind than unstructured sequences.[6,14–18] Additionally, the recognition mechanism of APOBEC proteins has been recently demonstrated to include sugar-specific interactions, effectively distinguishing against ssDNA and RNA.[19] HPLs are single stranded nucleic acid sequences which are able to fold and self-pair, and can have a small section of unpaired bases linking them to larger duplex DNA (see Fig. 1). HPLs are of increasing interest in pharmaceutical design, sensing, and targeted mutagenesis by subsequent cellular processes.[20–27] The highly tunable nature of hairpin loops arises from the complex interplay between stem binding affinity, loop size,[23] loop sequence,[24] and local environment.

The preferential activity upon hairpin loops suggests the possibility of "hotspot" sequences in DNA that may be preferred APOBEC3 substrates.[18] Bases in nucleic acid sequences are known to undergo flips (see Fig. 1) through rotation about the sugar-phosphate backbone, where they become oriented away from adjacent nucleobases.[28] The flipped-out base therefore has increased solvent exposure and reduced interference from adjacent nucleobases in active site binding. Furthermore, this "flipped out" conformation is known to be required for deamination activity, as it is the only way to bring the target cytosine within range of a reactive water in the active site. We hypothesize that
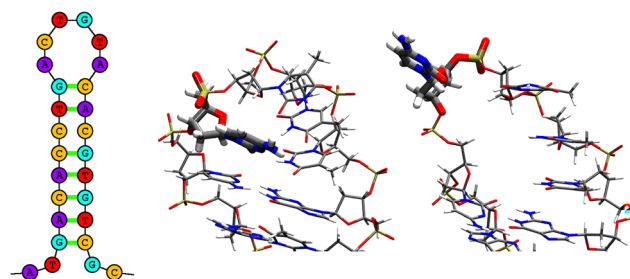
a Department of Chemistry, Wayne State University, 5101 Cass Ave., Detroit, MI 48202, USA. E-mail: arwalker@wayne.edu

b Department of Biochemistry, Microbiology and Immunology, Wayne State University School of Medicine, Detroit, MI 48201, USA

Fig. 1 An example of a hairpin loop (HPL) and nucleotide flipped in (left) and out (right) of an HPL.

these base flips must occur before substrate binding in order to facilitate deamination, and that there are observable physical characteristics related to specific hairpin sequences that may explain why certain sequences exhibit higher rates of base flipping.

The number of unique cytosine-containing sequences that may be obtained in an n-nucleotide loop is given by the formula $N_{unique} = 4^n - 3^n$. Therefore, a 3-nucleotide (3NT) loop yields 37 unique sequences, a 4NT loop yields 175, a 5NT loop yields 781, a 6NT loop results in 3367, and so on. As the number of sequences increases combinatorially, it becomes intractable and costly to experimentally test and analyze each sequence. Computational methods allow for large-scale screening of these unique hairpin sequences. Molecular dynamics (MD) simulations can provide insight into specific atomic-level motions of the HPLs, including base-flipping events, that can drive protein–substrate binding.

In this work we apply MD simulations to identify physical characteristics of loops which drive base-flipping events in solution, assess binding energies of cytosine-containing hairpin loops with APOBEC3A, compare to non-cytosine-containing loops with APOBEC3A, and demonstrate the potential release pathway of the product from the enzyme. We use unbiased MD on a relatively short timescale (100 ns per trajectory), and show that base-flipping is accessible and consistent on this timescale with replicate simulations. This allows us to comprehensively investigate all 3NT and 4NT loop sequences containing one cytosine, along with some additional non-cytosine containing loops for comparison.

2. Methods

2.1. DNA hairpins in solvent

We generated starting structures using Chimera v1.1635, creating a double-helix "stem" with the sequence 5′-TTAGCATG-AAA-CATGCTAA-3′, where the triadenine group acted as the template for the new hairpin loop sequences, and each base in the stem was paired.[29] All 3NT sequences containing at least one cytosine were generated from this initial structure by removing the nucleobase atoms from the template, renaming each nucleotide in the PDB file, and using the tleap program in AmberTools22[30] to regenerate the nucleotide based on standard atomic positions. This resulted in 37 unique 3NT loops containing at least one cytosine. The same method was also applied using the same stem sequence with an AAAA loop as the initial template structure for 4NT loops, which resulted in 175 unique 4NT sequences containing at least one cytosine. We also prepared the hairpins AGG, TTU and AAAA as non-cytosine containing examples for 3/4NT loops by the same method. Each initial structure for 3NT and 4NT loops was prepared for molecular dynamics simulation using the OL15 forcefield for DNA, TIP3P forcefield for solvent water, and the Joung Cheathem counterion parameters.[31,32] OL15 has been shown to have reasonable base-flipping dynamics for double helices.[28,33–43] We also ran several comparative trajectories with parm99bsc1.[44] Each system was neutralized with K^+ ions to a neutral charge, then solvated with TIP3P waters to a minimum distance of 20 Å between the nucleotide and the edge of the solvent box. We first minimized each system to eliminate potential bad contacts and clashes, then allowed the solvent box to equilibrate around restrained nucleotides. We heated each system iteratively, allowing the pressure to equilibrate at each 15 °C increment between 0 °C and 300 °C. Once each system was equilibrated with constant pressure, we performed classical molecular dynamics (MD) simulations with a Langevin thermostat (friction constant = 5 ps^{-1}) in an NVT ensemble at 300 °C and 1 atm using a 1 fs timestep for 100 ns of production using Amber22's pmemd.cuda module.[30] The electrostatic interactions were computed with particle mesh Ewald and the nonbonded interaction cutoff was set to 10 Å. The combined simulations of 212 unique hairpin loops in solvent yielded 21.2 μs of sampling.

2.2. Selected DNA hairpins bound to APOBEC3A

We extracted representative frames from the MD trajectories of selected sequences (ATC, CTC, TAC, TTC, ACGG, ATTC, GCAA, TTTC) which had the target cytosine base in both the "flipped-in" and "flipped-out" conformations. We also extracted frames from simulations of AGG and AAAA hairpins to act as non-cytosine-containing examples, allowing us to differentiate between interactions required for binding *versus* catalysis. These sequences were chosen to support future experimental work and provide a representative set. Additionally, we included the 3NT-HPL (TTU) system as a post-catalytic example. Each of these frames was overlaid on the crystal structure of APOBEC3A (PDB ID: 5KEG), which was selected since the crystal already included a bound DNA 4-mer which served as a guide for our own manual docking.[45] The existing tetramer was removed from the crystal after alignment, resulting in a new PDB which contained the protein and the extracted DNA hairpin bound in the active site. Upon release of AlphaFold3 (AF3), which added the ability to use machine learning methods to identify protein/nucleotide interfaces,[46] we also performed test calculations on ATC, CTC and ATTC sequences with AF3 to compare to the manual docking. The sequence of the crystallized protein includes two mutations (E72A, catalytically inactivating it, and C171A, to make the protein more soluble) which were not expected to significantly affect the ability of APOBEC3A to bind the target cytosine-containing motifs. Each protein/substrate complex was prepared for additional MD simulations in the same manner as above, and post-equilibration MD ran for 100 ns and five replicates, totaling 500 ns of sampling per system. The MD simulations of 12 unique sequences docked to APOBEC3A in both flipped-in and flipped-out orientations resulted in a total of 11.4 μs of sampling.

To obtain qualitative binding energies, we computed enthalpies *via* MM/GBSA with the MMPBSA.py program available in Amber22.[47] The absolute affinities cannot be compared directly with experimental values, as the affinity increases based on size of system and our obtained values are in the range of −10 to 100 kcal mol^{-1}. However, as previously noted with MM/GBSA methods, we do find that they qualitatively reproduce relative

binding affinity trends for our systems, given that they are sufficiently similar as with our sets of hairpin loops.[48]

3. Results and discussion

3.1. DNA hairpins in solution

**3.1.1. RMSD and sugar puckering metrics are base-agnostic.** The average root mean squared deviation (RMSD) over time was calculated for the target deoxycytidine (phosphate, sugar and base) over the course of the complete MD trajectory of each system. RMSD is used as an indicator of overall conformational stability of the target deoxycytidine in aqueous solution, with higher values indicating larger changes in orientation over time with respect to the starting structure. The sugar puckering of the deoxyribose ring of the deoxycytidine at each target position was calculated over time using the Altona-Sundaralingam method,[49] along with the average value. Time-resolved plots for each system can be found in the ESI.† Here, we use sugar puckering as a proxy to indicate the magnitude of change in the orientation of the target deoxycytidine with respect to the adjacent nucleotides in sequence. We first examined whether the individual values for RMSD or sugar puckering differed by position or nucleobase. We find that while the observed RMSD values vary from one position in the loop to the next, these values are generally consistent at each position regardless of which nucleobase is present (see Fig. 2). The sugar puckering is the property that shows sequence specificity, with values of 140–160° aligning with the flipped-out conformation and key high activity motifs, including 5′-T<u>C</u>-3′. This range overlaps the angular region defined as C2′-*endo*, which exhibits greater phosphate–phosphate distance across the nucleic acid backbone and allows for the base to easily flip from *anti* to *syn* conformations.[50] While the key positioning of the deoxycytidine for the APOBEC3s is known, these results suggest that combining sugar puckering

and RMSD values can be used to predict base-flipping behavior in DNA hairpins in general.

Recent work by Nakauma-González *et al.* identified several interesting trends related to "hot-spot" mutations on HPLs by APOBEC enzymes.[51] In that work, the authors illustrate that cytosines in the third or further position from the 5′ start of the HPL are frequently mutated by APOBECs. We observed in our simulations that bases at these positions exhibit a combination of higher RMSD values and maintain a narrower range of sugar pucker values, suggesting that base flips are more favorable in these positions and a possible relationship to the sequence-specificity of APOBEC enzymatic activity. By comparison, bases in other positions with lower RMSD values exhibit a broader range of sugar pucker values. Together, this suggests that base flips may be less favorable at positions closer to the stem of the HPL as the phosphate bonds are less able to rotate, causing the deoxyribose to explore a larger conformational space instead.

3.2. DNA hairpins in complex with APOBEC3A

3.2.1. Bound hairpins cannot undergo base flips. To determine the relationship between base flipping and APOBEC3A binding, we extracted representative frames from the GCAA sequence dynamics in both flipped-in and flipped-out orientations. These structures were overlaid onto the existing DNA 4-mer in the 5KEG crystal structure of APOBEC3A. The DNA 4-mer was subsequently removed to generate the initial pre-docked enzyme-substrate complex. After MD simulations were complete, we examined the position of the target cytosine relative to the active site over the course of the entire trajectory. The flipped-out orientation of the target cytosine in the GCAA sequence remained stable in the active site during the simulation (see Fig. 3a). Conversely, when the cytosine is flipped into the hairpin docked to the enzyme, the cytosine is significantly
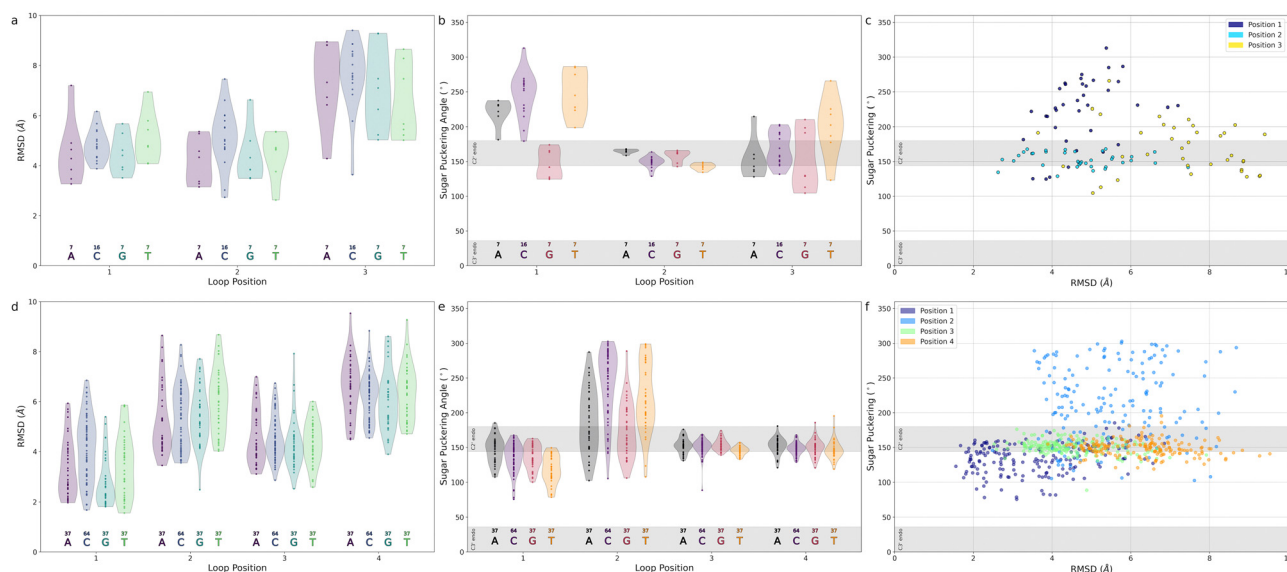
Fig. 2 (top) Trimer HPLs (a) average RMSD of each base at each position, (b) average sugar puckering of each base and position, (c) comparison of RMSD and sugar puckering grouped by position. (bottom) Tetramer HPLs (d) average RMSD of each base at each position in a tetramer HPL, (e) average sugar puckering of each base and position, and (f) comparison of RMSD and sugar puckering grouped by position.
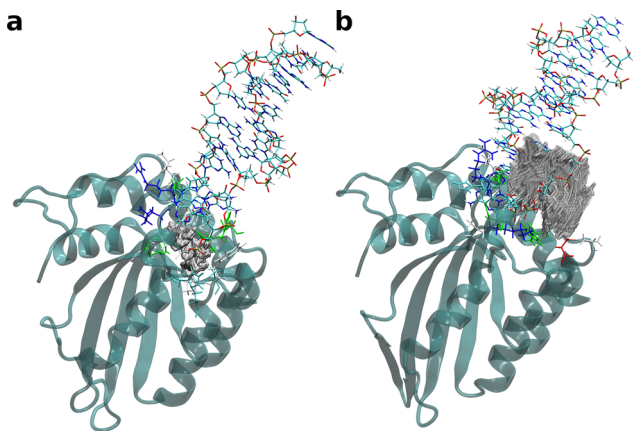
Fig. 3 HPL with GCAA loop sequence docked to APOBEC3A active site in (a) flipped-out and (b) flipped-in orientations. Grey structures represent target cytosine at all timesteps of simulation relative to active site position.

more mobile during the simulation (see Fig. 3b). Interestingly, despite this increase in mobility, there appears to be no available conformational pathways which allow the flipped-in cytosine to enter the active site for reactivity without unbinding.

Additional simulations were performed with 3NT sequences ATC, CTC, GTC, TTC, and TAC. Similar behaviors were observed in sequences in which the cytosine was initially flipped into the hairpin loop, most notably the higher level of mobility and the inaccessibility of the active site. By contrast to the larger 4NT sequences, the 3NT sequences which began flipped out of the loop and bound in the active site exhibited lower stability as well, with somewhat more flexibility and motion in the active site itself (see Fig. 4). However, as with the 4NT sequence, none of the 3NT sequences were able to bind or unbind from the active site in opposition to their starting orientation, again indicating that once bound, DNA sequences are not able to undergo base-flipping events which will allow cytosine to enter the active site. This further supports our hypothesis that hairpin loops must undergo base-flip events in solvent before protein binding in order to allow for the deamination reaction to proceed.

3.3. Cytosine is not necessary for A3A/HPL binding

To determine if the native cytosine substrate was necessary for binding, we performed additional simulations on hairpin sequences which did not contain cytosine (AGG and AAAA), then repeated
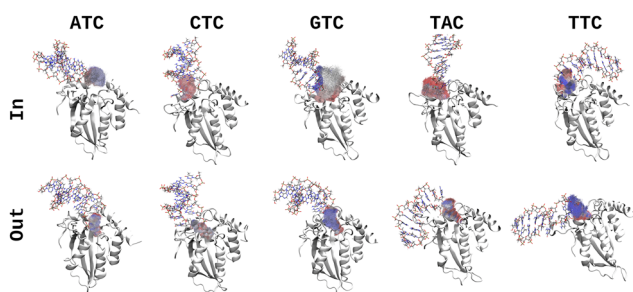
binding simulations and analyses as above. For the 3NT loop AGG, we selected frames based on the base-flipped conformation of the 3′ guanine to be consistent with the cytosine-containing 3NT sequences. For the 4NT loop AAAA, we selected frames based on the second loop position, consistent with GCAA above. The AGG loop exhibits similar behavior to the GTC and TAC sequences, with the flipped-out initial configuration showing reduced binding affinity compared to the flipped-in. By contrast, the AAAA loop appears to have much stronger binding affinity when the nucleotide is in the active site. We attribute these disparities to the respective functional groups of the different nucleotides. The carbonyl group of the guanine is analogous to the uracil which would be present after successful deamination, while the amine group of the adenine mimics that of the cytosine. With these structural features in mind, it is reasonable to expect an enzyme would exhibit reduction in binding favorability with the the product of its catalyzed reaction, as this would encourage dissociation and subsequently free the binding site for further catalysis. The AAAA loop functions similarly to the TTU disfavored binding and eventual unbinding pathway, as discussed above.

3.4. Base flips prior to binding determine binding affinity

In order to relate sequence to binding affinity more directly, we calculated binding affinities for several hairpin sequences in APO-BEC3A using MM/GBSA. These binding energies include the entire hairpin sequence (19 nucleotides for 3NT loops) against the entire receptor complex (188 amino acids, 1 Zn^{2+} ion, and 1 coordinated water). Each trajectory was analyzed via a bootstrapping method and the resulting binding energies compared across all systems (see Fig. 5). For the ATC, CTC, and TAC sequences, the flipped-out conformations have more favorable binding energies than their flipped-in counterparts, while the opposite is true for the GTC and TTC sequences. However, the difference in favorability is considerably smaller for the GTC/TTC sequences as compared to ATC/CTC/ TAC, supporting the idea that base-flipping generally improves binding. In examining the 4NT loops, we find that all tested sequences exhibit tighter binding after base-flipping than to their unflipped counterparts. Given that the phosphate backbone is able to interact with positively charged surface residues near the active site in both conformations, the difference is likely driven by favorable interactions with active site residues involved in the catalytic process.
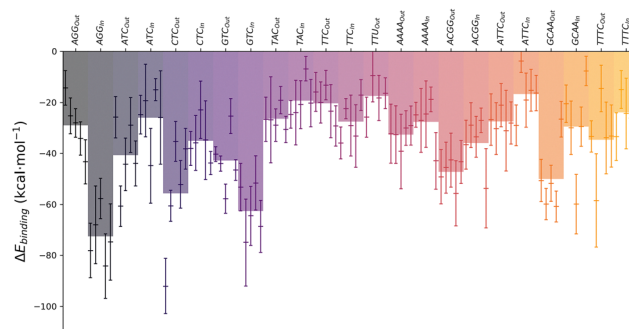

Fig. 4 Dynamic motions of selected 3NT sequences docked to APO-BEC3A in flipped-in and flipped-out conformations.

Fig. 5 Binding energies (MMGBSA) for selected sequences docked to APOBEC3A in flipped-in and flipped-out conformations.

3.5. Uracilated loops exhibit lower binding energies

To mimic the system after uracilation, we modified the final frame of the TTC-containing HPL docked to APOBEC3A by mutating the cytosine to uracil. We then performed MD to compare how going from reactant to product for catalysis affected substrate binding. We compared nearby residues in the first and last frame of the product (TTU) HPL and noted that many critical interactions which were present for the entire reactant (TTC) simulation were lost (see Fig. 6). The orientation of H61 changed during the unbinding of TTU, with K21 and K51 stabilizing the phosphate backbone as the HPL begins to move away from the active site. At this point R19 is able to engage with the HPL and continue guiding it away from the active site. At the start of the TTU simulation, the uracil is 4.15 Å from the α-carbon of H61, moving to 6.82 Å by the end. As shown in Fig. 5, the TTU sequence exhibits less favorable binding than the TTC motif. These motions are likely crucial for substrate release post-catalysis.

3.6. Manually docked systems are closely matched by AlphaFold3 models

We compared the results of the manually docked ATC-containing hairpin loop to APOBEC3A with those provided by AlphaFold3 and found that there is good agreement between the systems (see Fig. 7). Specifically, the protein structure is highly conserved between the two systems, AlphaFold3 correctly identifies the nucleotide sequence as a hairpin, identifies the target cytosine in the hairpin loop, and properly flips the base into the active site. The major difference is visible only in
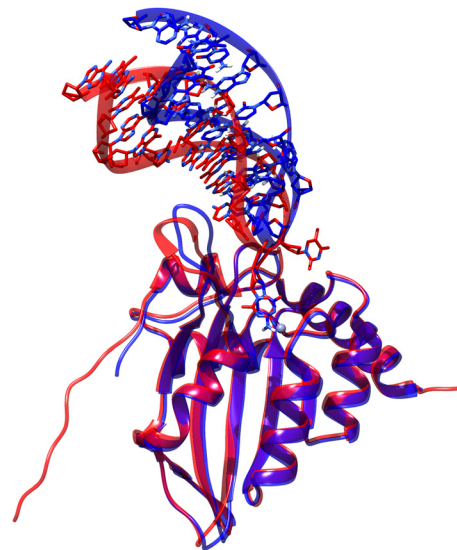

Fig. 7 Comparison of manually docked ATC-containing sequence with APOBEC3A (blue) and results of AlphaFold3 provided with sequences of protein and nucleotide only (red). Notably, the protein structures are almost exactly conserved, the nucleotide sequence is correctly identified as a hairpin loop, and the target cytosine is correctly identified, flipped out of the loop, and docked into the active site of APOBEC3A.

the exact direction in which the hairpin stem extends into solvent. However, during MD simulations this direction is highly mobile, and the AF3 prediction is within its typical range of motion. Therefore, future works to dock hairpin loops to APOBEC3A may be made significantly simpler by using Alpha-Fold3 rather than performing classical dynamics on solvated loops and manually docking representative frames.

3.7. DNA forcefield selection may impact observed dynamics in free nucleotide simulations

We performed test simulations on the ATC hairpin loop using OL21[52] and parmbsc1[44] forcefields to compare against OL15 used in this study. In comparing the resulting simulations, we find that OL21 produces dynamics similar to those from OL15, with comparable base-flipping behavior and nucleotide backbone motion. By contrast, the parmbsc1 simulation exhibits a highly constrained backbone with considerably less base-flipping behavior at the cytosine position. Interestingly, the 5′ thymine flips out of the hairpin loop early in the simulation and remains exposed for the duration. Meanwhile, the cytosine appears to pi-stack with the adenine in the hairpin and remain in that configuration throughout the simulation. Given this difference in base-flipping behavior and apparent rigidity of the phosphate backbone with parmbsc1, we are confident in our selection of the OL15 forcefield used for this study.

4. Conclusions

Simulating hairpin loop motion in solvent can provide insights into the physical drivers of base-flipping events, providing a pathway to relate large-scale sequence data to APOBEC
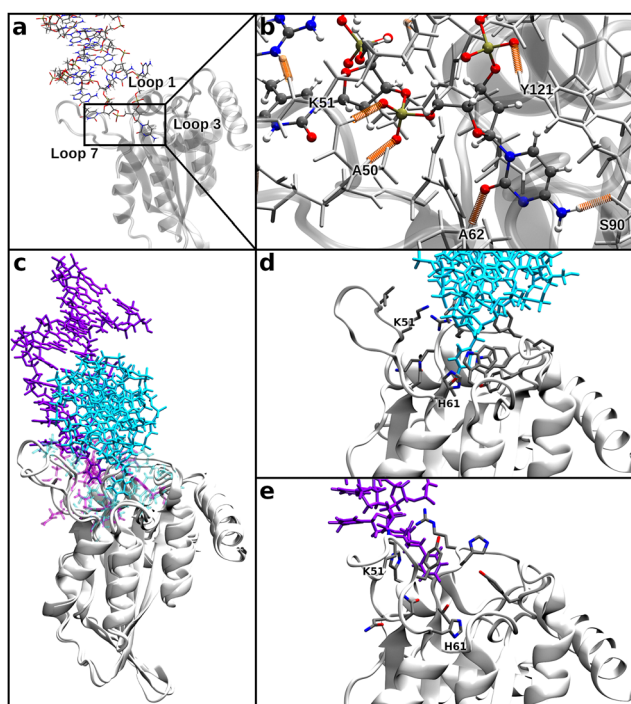

Fig. 6 (a) Initial binding orientation of TTC HPL in APOBEC3A, (b) critical protein–substrate interactions on binding, (c) first and last frame of TTU HPL in APOBEC3A, (d) zoomed in active site of first frame for TTU HPL, and (e) zoomed in active site of last frame of TTU HPL.

substrate preferences. In this work, we have generated a complete set of 3NT and 4NT hairpin loops, investigated their dynamics with relatively short timescale unbiased MD (100 ns per trajectory), and provided insights with both a manually and AF3-docked subset of these loops to demonstrate the physical connection between base-flipping and substrate binding. We find that 100 ns is sufficient to see multiple base-flipping events and to differentiate between hairpin loop sequences that are preferred by APOBEC3A. We note that choice of force field can affect these results, but that OL15 has been shown to successfully replicate base-flips in duplex DNA in previous work, even with nonstandard DNA bases.[40,53] We also find that while MM/GBSA will not accurately compute the absolute free energies for the hairpin loops bound to APOBEC3A, their relative ordering by affinity is consistent with experimental biochemical data for hairpin loop preferences. The use of sugar puckering and RMSD provide guidance for the prediction of base-flipping events, which in turn correlate with binding energies of HPL to APOBEC3A. We find that while cytosine is required for deamination to uracil, it is not necessary for binding to APOBEC3A. We also find that base-flipping of a nucleotide in a hairpin loop must occur before binding in order to facilitate the subsequent enzyme catalysis.

Author contributions

M. A. H. performed free-hairpin molecular dynamics simulations, complexed simulations, and analyses. P. G. performed additional complexed simulations and related analyses. A. S. B. initiated the project, contributed to the discussion of ideas and data, and provided biological expertise. A. R. W. supervised and directed the work and provided computational resources and funding.

Data availability

CSV files containing RMSD and sugar puckering data for all free nucleotide simulations may be found at https://doi.org/10.5281/zenodo.13256543. Graphs of RMSD and sugar puckering data, including replicates, can be found in the ESI.†

Conflicts of interest

The authors have no conflicts to declare.

Acknowledgements

Notes and references

1 L. Chelico, P. Pham, P. Calabrese and M. F. Goodman, *Nat. Struct. Mol. Biol.*, 2006, **13**, 392–399.

2 L. Chelico, C. Prochnow, D. A. Erie, X. S. Chen and M. F. Goodman, *J. Biol. Chem.*, 2010, **285**, 16195–16205.

3 Y. N. Lee, M. H. Malim and P. D. Bieniasz, *J. Virol.*, 2008, **82**, 8762–8770.

4 S. G. Conticello, *Genome Biol.*, 2008, **9**, 229.

5 M. A. Carpenter, E. Rajagurubandara, P. Wijesinghe and A. S. Bhagwat, *DNA Repair*, 2010, **9**, 579–587.

6 K. Shi, M. A. Carpenter, S. Banerjee, N. M. Shaban, K. Kurahashi, D. J. Salamango, J. L. McCann, G. J. Starrett, J. V. Duffy, O. Demir, R. E. Amaro, D. A. Harki, R. S. Harris and H. Aihara, *Nat. Struct. Mol. Biol.*, 2017, **24**, 131–139.

7 M. Liu, A. Mallinger, M. Tortorici, Y. Newbatt, M. Richards, A. Mirza, R. L. Van Montfort, R. Burke, J. Blagg and T. Kaserer, *ACS Chem. Biol.*, 2018, **13**, 2427–2432.

8 D. Ebrahimi, H. Alinejad-Rokny and M. P. Davenport, *PLoS One*, 2014, **9**, 1–9.

9 A. Rathore, M. A. Carpenter, O. Demir, T. Ikeda, M. Li, N. M. Shaban, E. K. Law, D. Anokhin, W. L. Brown, R. E. Amaro and R. S. Harris, *J. Mol. Biol.*, 2013, **425**, 4442–4454.

10 E. C. Logue, N. Bloch, E. Dhuey, R. Zhang, P. Cao, C. Herate, L. Chauveau, S. R. Hubbard and N. R. Landau, *PLoS One*, 2014, **9**, 1–10.

11 R. M. Kohli, R. W. Maul, A. F. Guminski, R. L. McClure, K. S. Gajula, H. Saribasak, M. A. McMahon, R. F. Siliciano, P. J. Gearhart and J. T. Stivers, *J. Biol. Chem.*, 2010, **285**, 40956–40964.

12 J. A. Bohn, K. Thummar, A. York, A. Raymond, W. C. Brown, P. D. Bieniasz, T. Hatziioannou and J. L. Smith, *Nat. Commun.*, 2017, **8**, 1021.

13 Y. Feng, R. P. Love, A. Ara, T. T. Baig, M. B. Adolph and L. Chelico, *J. Biol. Chem.*, 2015, **290**, 27188–27203.

14 A. Langenbucher, D. Bowen, R. Sakhtemani, E. Bournique, J. F. Wise, L. Zou, A. S. Bhagwat, R. Buisson and M. S. Lawrence, *Nat. Commun.*, 2021, **12**, 1602.

15 L. Wong, A. Sami and L. Chelico, *Nucl. Acids Res.*, 2022, **50**, 12039–12057.

16 R. Buisson, A. Langenbucher, D. Bowen, E. E. Kwan, C. H. Benes, L. Zou and M. S. Lawrence, *Science*, 2019, **364**, eaaw2872.

17 A. L. Brown, C. D. Collins, S. Thompson, M. Coxon, T. M. Mertz and S. A. Roberts, *Sci. Rep.*, 2021, **11**, 21008.

18 R. Pecori, S. Di Giorgio, J. Paulo Lorenzo and F. Nina Papavasiliou, *Nat. Rev. Genet.*, 2022, **23**, 505–518.

19 M. K. Wyllie, C. K. Morris, N. H. Moeller, H. A. M. Schares, R. Moorthy, C. A. Belica, M. J. Grillo, Ö. Demir, A. M. Ayoub, M. A. Carpenter, H. Aihara, R. S. Harris, R. E. Amaro and D. A. Harki, *ACS Chem. Biol.*, 2025, **20**, 117–127.

20 H. Zahraee, Z. Khoshbin, F. Mohammadi, M. Mashreghi, K. Abnous and S. M. Taghdisi, *Trends Anal. Chem.*, 2023, **165**, 117160.

21 K. Deiorio-Haggar, J. Anthony and M. M. Meyer, *RNA Biol.*, 2013, **10**, 1180–1184.

22 Y. Shen, S. V. Kuznetsov and A. Ansari, *J. Phys. Chem. B*, 2001, **105**, 12202–12211.

23 I. Prislan, H.-T. Lee, C. Lee and L. A. Marky, *J. Phys. Chem. B*, 2015, **119**, 96–104.

24 L. E. Xodo, G. Manzini, F. Quadrifoglio, G. Van Der Marel and J. Van Boom, *Nucl. Acids Res.*, 1991, **19**, 1505–1511.

25 B. Nguyen and W. D. Wilson, *J. Phys. Chem. B*, 2009, **113**, 14329–14335.

26 N. E. Broude, K. Woodward, R. Cavallo, C. R. Cantor and D. Englert, *Nucl. Acids Res.*, 2001, **29**, e92.

27 G. Wang and K. M. Vasquez, *Nat. Rev. Genet.*, 2023, **24**, 211–234.

28 Nicy, D. Chakraborty and D. J. Wales, *J. Phys. Chem. B*, 2022, **126**, 3012–3028.

29 E. F. Pettersen, T. D. Goddard, C. C. Huang, G. S. Couch, D. M. Greenblatt, E. C. Meng and T. E. Ferrin, *J. Comput. Chem.*, 2004, **25**, 1605–1612.

30 D. A. Case, T. E. Cheatham, T. Darden, H. Gohlke, R. Luo, K. M. Merz, A. Onufriev, C. Simmerling, B. Wang and R. J. Woods, *J. Comput. Chem.*, 2005, **26**, 1668–1688.

31 M. Zgarbová, J. Šponer, M. Otyepka, T. E. I. Cheatham, R. Galindo-Murillo and P. Jurečka, *J. Chem. Theory Comput.*, 2015, **11**, 5723–5736.

32 W. L. Jorgensen, J. Chandrasekhar, J. D. Madura, R. W. Impey and M. L. Klein, *J. Chem. Phys.*, 1983, **79**, 926–935.

33 D. Sharma, K. Sharma, A. Mishra, P. Siwach, A. Mittal and B. Jayaram, *Phys. Chem. Chem. Phys.*, 2023, **25**, 7323–7337.

34 G. Kudo, T. Hirao, R. Harada, T. Hirokawa, Y. Shigeta and R. Yoshino, *Sci. Rep.*, 2024, **14**, 13508.

35 C. Selvaraj, U. Panwar, D. C. Dinesh, E. Boura, P. Singh, V. K. Dubey and S. K. Singh, *Front. Chem.*, 2021, **8**, 595273.

36 J. C. Flores-Canales, N. A. Simakov and M. Kurnikova, Microsecond Molecular Dynamics Simulations of Diphtheria Toxin Translocation T-Domain pH-Dependent Unfolding in Solution, *biorxiv*, preprint, 2019, DOI: 10.1101/572040.

37 H. Kim and Y. Pak, *J. Chem. Inf. Model.*, 2024, **64**, 4511–4517.

38 F. Pan, Y. Zhang, V. H. Man, C. Roland and C. Sagui, *Nucl. Acids Res.*, 2018, **46**, 942–955.

39 Z. Sun and J. Z. Zhang, *CCS Chem.*, 2021, **3**, 1026–1039.

40 Z. Sun, X. Wang, J. Z. H. Zhang and Q. He, *Phys. Chem. Chem. Phys.*, 2019, **21**, 14923–14940.

41 X. Wang and Z. Sun, *J. Chem. Inf. Model.*, 2019, **59**, 2980–2994.

42 Y. Z. Chen, V. Mohan and R. H. Griffey, *Phys. Rev. E: Stat. Phys., Plasmas, Fluids, Relat. Interdisc. Top.*, 2000, **62**, 1133–1137.

43 R. Galindo-Murillo, J. C. Robertson, M. Zgarbová, J. Šponer, M. Otyepka, P. Jurečka and T. E. Cheatham, *J. Chem. Theory Comput.*, 2016, **12**, 4114–4127.

44 I. Ivani, P. D. Dans, A. Noy, A. Pérez, I. Faustino, A. Hospital, J. Walther, P. Andrio, R. Goñi, A. Balaceanu, G. Portella, F. Battistini, J. L. Gelpí, C. González, M. Vendruscolo, C. A. Laughton, S. A. Harris, D. A. Case and M. Orozco, *Nat. Meth.*, 2016, **13**, 55–58.

45 T. Kouno, T. V. Silvas, B. J. Hilbert, S. M. D. Shandilya, M. F. Bohn, B. A. Kelch, W. E. Royer, M. Somasundaran, N. Kurt Yilmaz, H. Matsuo and C. A. Schiffer, *Nat. Commun.*, 2017, **8**, 15024.

46 J. Abramson, J. Adler, J. Dunger, R. Evans, T. Green, A. Pritzel, O. Ronneberger, L. Willmore, A. J. Ballard, J. Bambrick, S. W. Bodenstein, D. A. Evans, C.-C. Hung, M. ONeill, D. Reiman, K. Tunyasuvunakool, Z. Wu, A. Žemgulytė, E. Arvaniti, C. Beattie, O. Bertolli, A. Bridgland, A. Cherepanov, M. Congreve, A. I. Cowen-Rivers, A. Cowie, M. Figurnov, F. B. Fuchs, H. , Gladman, R. Jain, Y. A. Khan, C. M. R. Low, K. Perlin, A. Potapenko, P. Savy, S. Singh, A. Stecula, A. Thillaisundaram, C. Tong, S. Yakneen, E. D. Zhong, M. Zielinski, A. Žídek, V. Bapst, P. Kohli, M. Jaderberg, D. Hassabis and J. M. Jumper, *Nature*, 2024, **630**, 493–500.

47 B. R. I. Miller, T. D. J. McGee, J. M. Swails, N. Homeyer, H. Gohlke and A. E. Roitberg, *J. Chem. Theory Comput.*, 2012, **8**, 3314–3321.

48 S. Genheden and U. Ryde, *Expert Opin. Drug Discovery*, 2015, **10**, 449–461.

49 C. Altona and M. Sundaralingam, *J. Am. Chem. Soc.*, 1973, **95**, 2333–2344.

50 P. S. Ho and M. Carter, in *DNA Structure: Alphabet Soup for the Cellular Soul*, ed. H. Seligmann, IntechOpen, Rijeka, 2011, ch. 1.

51 J. A. Nakauma-González, M. Rijnders, M. T. Noordsij, J. W. Martens, A. A. Van Der Veldt, M. P. Lolkema, J. L. Boormans and H. J. Van De Werken, *Cell Genom.*, 2024, **4**, 100528.

52 M. Zgarbová, J. Šponer and P. Jurečka, *J. Chem. Theory Comput.*, 2021, **17**, 6292–6301.

53 O. Love, R. Galindo-Murillo, M. Zgarbová, J. Šponer, P. Jurečka and T. E. I. Cheatham, *J. Chem. Theory Comput.*, 2023, **19**, 4299–4307.